View Article Online
View Journal

Green Chemistry

Cutting-edge research for a greener sustainable future

Accepted Manuscript

This article can be cited before page numbers have been issued, to do this please use: B. S. K. Jayantha, R. Summers, . Zhang, G. P. Mendis and L. N. Jayakody, *Green Chem.*, 2025, DOI: 10.1039/D5GC02883C.

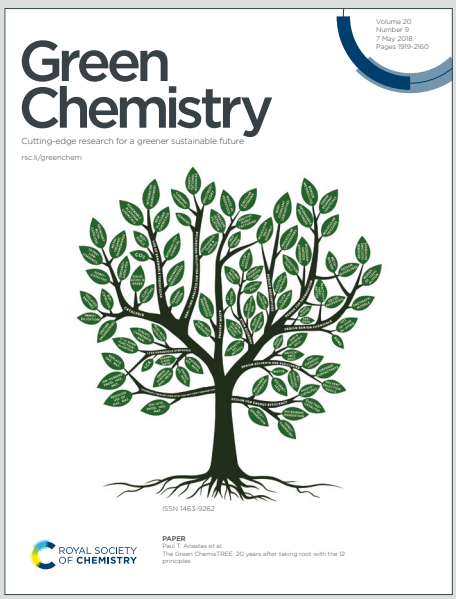

View Article Online
DOI: 10.1039/D5GC02883C

Green Foundation

1. The article presents an engineered monoculture of *Pseudomonas putida*, which serves as a biocatalytic system for the efficient and eco-friendly production of pharmaceutical-grade methylated xanthines from caffeine, achieving a 100% yield (highly selective conversion) compared to traditional low-specific chemical synthesis.

2. Our approach replaces hazardous chemical synthesis for methylated xanthines with a biocatalytic system and repurposes glycerol, a waste product from biodiesel production. This renewable feedstock-based green method has achieved a yield of 9.2±0.42 g/L of 7-MX, the highest concentration from caffeine in a bioreactor at 30°C, with low E-factor and PMI values, indicating minimal environmental impact.

3. Incorporating solid caffeine into the reactor and enhancing biocatalysts to withstand caffeine toxicity can reduce water usage, lower the carbon footprint, and cut production costs. Developing a solvent-free *in-situ* separation process for product recovery can further minimize environmental impact.

View Article Online
DOI: 10.1039/D5GC02883C

ARTICLE

Received 00th January 20xx,
Accepted 00th January 20xx

DOI: 10.1039/x0xx00000x

Engineered *Pseudomonas putida* monoculture system for green synthesis of 7-methylxanthine

Bhagya Jayantha[a], Shuyuan Zhang[b], Ryan M. Summers[b], Gamini P. Mendis[c], Lahiru N. Jayakody[a,d]*

7-methylxanthine (7-MX) is a clinically proven safe drug to treat myopia. The chemical synthesis of 7-MX is hindered due to low specificity, demanding sustainable biological production using renewable, cost-effective feedstocks. To this end, we systematically engineered robust *P. putida* EM42 to produce 7-MX using caffeine and glycerol in minimal salt media. Removing transcriptional repressor (*glpR*), genome integration of heterologous *N*-demethylase and its reductase, *ndmABD*, and overexpression of native *fdhA* to balance the redox cofactors enabled the selective conversion of caffeine to 7-MX with 100% yield. We discovered a native transporter, *PP_RS18750*, that efficiently uptakes caffeine, facilitating the conversion in glycerol-containing media. We achieved 9.2±0.42 g/L of 7-MX in a 3-L bioreactor by process-level optimization, the highest titer reported to date. Our techno-economic analysis indicates that this novel engineered monoculture approach can produce pharmaceutical-grade 7-MX commercially for $328/kg, with remarkably low E-factor and Process Mass Intensity (PMI) values, demonstrating the sustainable green valorization of caffeine into high-value methylated xanthine.

[a] *School of Biological Science, Southern Illinois University Carbondale. Carbondale, Illinois,*
[b] *Department of Chemical and Biological Engineering, The University of Alabama, Tuscaloosa, AL, USA*
[c] *School of Engineering, Penn State University, Erie, PA, USA*
[d] *Fermentation Science Institute, Southern Illinois University Carbondale. Carbondale, Illinois, USA. e-mail: Lahiru.jayakody@siu.edu*

View Article Online
DOI: 10.1039/D5GC02883C

Green Foundation

1. The article presents an engineered monoculture of *Pseudomonas putida*, which serves as a biocatalytic system for the efficient and eco-friendly production of pharmaceutical-grade methylated xanthines from caffeine, achieving a 100% yield (highly selective conversion) compared to traditional low-specific chemical synthesis.

2. Our approach replaces hazardous chemical synthesis for methylated xanthines with a biocatalytic system and repurposes glycerol, a waste product from biodiesel production. This renewable feedstock-based green method has achieved a yield of 9.2±0.42 g/L of 7-MX, the highest concentration from caffeine in a bioreactor at 30°C, with low E-factor and PMI values, indicating minimal environmental impact.

3. Incorporating solid caffeine into the reactor and enhancing biocatalysts to withstand caffeine toxicity can reduce water usage, lower the carbon footprint, and cut production costs. Developing a solvent-free *in-situ* separation process for product recovery can further minimize environmental impact.

1.0 Introduction

Methylxanthines are used to treat a variety of diseases and disorders, including myopia [1-3]. Myopia is rapidly increasing globally, with projections suggesting that by 2050, half of the world's population will be affected [2]. 7-methylxanthine (7-MX), an adenosine antagonist, can enhance collagen-related amino acids in the sclera and increase collagen fibril diameter to reduce myopia progression. Approved by the Danish Medicines Agency in 2009, 7-MX is recognized as a safe and effective oral therapy for managing myopia in children [4]. Clinical studies show that children aged 8 -15 given 400 mg of 7-MX twice daily showed reduced myopia progression by nearly 60% [2]. In addition, 7-MX can cross the blood-brain barrier, making it useful for developing compounds like (E)-8-(3,4-dimethoxystyryl)-1,3-dipropyl-7-MX, a potent antagonist of the A2 adenosine receptor, and 1,3-dipropyl-7-methylxanthine to induce apoptosis of lung carcinoma cells [5].

7-MX is limited in natural availability and is only present as an intermediate of caffeine biosynthesis in plants [6]. Chemical methods of synthesis, such as solution phase syntheses, solid-phase synthesis, Traube process, and N-substitution of Xanthines, are used to address its limited natural availability [7-10]. Generally, solution-phase synthesis requires multistep reactions and tedious chromatographic separations. Solid-phase processes involve hazardous chemicals, such as tetrahydrofuran (THF), Dimethylaminopropylamine (DMAP), and N, N-dimethylformamide (DMF) [8, 11, 12]. Traube purine synthesis remains the most widely used chemical process, yet is constrained by being lengthy, requiring harsh conditions, and lacking purity, even with its recent modifications [10, 11, 13]. Direct N-substitution of xanthine is complicated due to the lack of selectivity of N_3-H and N_7-H, closely followed by N_1-H. A biosynthetic route that converts caffeine (1,3,7-trimethylxanthine) to 7-methylxanthine. Collectively, poor specificity, complicated synthetic process, and the use of hazardous chemicals hinder the chemical manufacturing of 7-MX [13, 14].

As an alternative, researchers have demonstrated the sustainable and selective biosynthesis of 7-MX by harnessing *N*-demethylation enzymes from *Pseudomonas putida* CBB5 (hereafter referred to as CBB5), , which enables the conversion of caffeine to xanthine [15]. Researchers established the reaction mechanism of N-demethylase enzymes via detailed biochemical studies and computational modelling [16]. The NdmA and NdmB enzymes are Rieske nonheme iron monooxygenases that remove the methyl groups from caffeine's N1 and N3 positions, respectively. NdmC is a nonheme iron monooxygenase that removes the N7-methyl

View Article Online
DOI: 10.1039/D5GC02883C

group from 7-MX to form xanthine. All these reactions are dependent upon the Rieske reductase, NdmD which is a partner reductase that transfers electrons from nicotinamide adenine dinucleotide (NADH) to power the reaction [16]. NdmE is a structural subunit that connects NdmC and NdmD, completing the final N-demethylation step to form xanthine [17]. Recent studies have reported on the production of 7-MX and related methylxanthines from caffeine by plasmid-based expression of NdmABD in *Escherichia coli* as host.[13, 14, 18, 19] For instance, Mock and co-workers have produced about 2.1 mM of 7-MX from 4.3 mM of caffeine using a monoculture expressing NdmABD. A coculture of NdmAD and NdmBD enables 97% conversion of caffeine to achieve a maximum titer of 2.3 mM of 7-MX [13, 14]. The most recent report on the redox-engineered *E. coli* BW25113 strain produced 50.35 mM[18]. Notably, the process requires transferring the rich media-grown cells to the buffer media for the conversion step and very high cell density (OD_{600}=100) to achieve the titer. The strain requires antibiotics to maintain the plasmids and inducers for gene expression. None of the previous studies investigated host strains other than *E. coli* and alternate, less expensive co-carbon sources for 7-MX production.

Pseudomonas putida KT2440 (hereafter referred to as KT2440),is a non-pathogenic and metabolically robust bacterium with well-developed genetic tools for engineering new synthetic pathways, and it has been successfully engineered to produce a wide variety of new products from both conventional and non-conventional feedstocks [20]. The genome-reduced strain *P. putida* EM42 (hereafter referred to as EM42),demonstrates significant tolerance to chemicals due to its high ATP and redox potential compared to the parental strain, KT2440 [21]. Notably, this strain has been engineered for the utilization and bio-valorization of highly toxic chemical feedstocks [22]. In this report, we describe the development of an efficient, industrially applicable genome-engineered EM42 that selectively produces 7-MX from caffeine, achieving nearly 100% yield. We identified the native caffeine transporter that allows for efficient caffeine utilization in the engineered strain when grown in minimal salt media (M9) supplemented with glycerol (a by-product of biodiesel) as the sole carbon source. Systematic strain engineering, optimization for redox balance, and process-level improvements have enabled us to produce the highest titer of 7-MX, ~58 mM to date, making this strain the most efficient for the green and economically feasible production of pharmaceutical-grade 7-MX.

2.0 Experimental section

2.1 Materials

Caffeine (>98.0%), theobromine (>98%), Paraxanthine (>98%), and theophylline (>98%) were purchased from TCI C0., LTD and 7-MX (>98%) from Thermo Scientific. Glycerol (>99.5%) was acquired from FisherBiotech. HPLC grade Methanol for the HPLC analysis and ethyl acetate for extraction were acquired from Fisher Chemical TM.

2.2 Plasmid construction

Q5 HotStart High-Fidelity2×MasterMix (New England Biolabs) and primers synthesized by Integrated DNA Technologies (IDT) were used in all PCR amplifications. Plasmids were constructed using Hi-Fi DNA assembly (New England Biolabs) according to the manufacturer's instructions. Primers used for PCR amplification are listed in **Table S1.** The plasmid, pBTL-2, was used as the backbone of all plasmid-based overexpression constructs. Features such as promoters and terminators are depicted in **Fig. S1-S7.** Plasmids were constructed by amplifying the plasmid (pBLT-2) and gene(s) of interest from EM42 and CBB5. Primers used in sequence confirmations of plasmids are listed in **Table S2**.

Gene integrations were done by plasmids constructed in sK18sB, which is unable to replicate in EM42 and contains the kanamycin-resistant marker to select for integration of the

plasmid into the genome by homologous recombination and *sacB* to counter-select for a second recombination event to remove the plasmid backbone from the genome subsequently [22].

2.3 Strain construction

The plasmid-based strains were generated by transforming respective plasmids into the DH5α-*Iq* strain of *E. coli* as described in Franden et al., (2018)[23]. The transformed bacteria were spread on LB agar medium supplemented with antibiotics. The transformation mixture was then kept at 37 °C overnight. Clones were screened using colony polymerase chain reaction (PCR), and plasmids from the positive clones were extracted, amplified, and sequenced for further validation. The plasmids from the successfully constructed clones were extracted and then transformed into EM42 competent cells, yielding the engineered plasmid-based strains used in this study.

EM42 was used as the basis of strain engineering and gene replacements were made using the *sacB* system of selection and counter-selection. To prepare electro-competent cells of different EM42 strains, we have used the protocol from Franden et al., (2018)[23]. Briefly, cultures were grown overnight in LB broth and incubated at 30 °C, shaking at 250 rpm. The next day, cells were centrifuged at 4500 rpm for 5 min at room temperature and washed three times in 300 mM sucrose in half the original volume. Finally, the cells were resuspended in 1/50th of the culture's original volume in 300 mM sucrose. Plasmid transformation was performed by introducing 5 µL (200 ng – 1 µg) of plasmid DNA to 50 µL of the electrocompetent cells, transferred to a chilled 0.1 cm electroporation cuvette, and electroporated at 1.6 kV, 25 µF, and 200 Ω. Subsequently, 950 µL SOC (NEB) was added and the cells were incubated with shaking at 250 rpm, 30 °C, for 1.5 h. 200 µL of transformation mix was plated on an LB agar plate containing appropriate antibiotics and incubated at 30 °C overnight.

For sucrose counter-selection, clonal transformants were streaked on YT plates containing 30% (w/v) sucrose (10 g/L yeast extract, 20 g/L tryptone, 250 g/L sucrose, 18 g/L agar), and incubated at 30 °C overnight. EM42 containing the *sacB* gene cannot grow on YT+30% (w/v) sucrose media. Therefore, single colonies presumed to have lost the *sacB* gene via homologous recombination, indicated by larger colonies, were picked and re-streaked on fresh YT+30% (w/v) sucrose plates and incubated at 30 °C overnight to finally obtain clonal sucrose-resistant and antibiotic-sensitive strains. All strains were analyzed for the correct gene replacement by performing a colony PCR at the site of integration. **Table S3** lists the specific strains produced in this work and the plasmids used for the integration. **Table S4** lists the primers used in sequence confirmation of genome-integrated/deleted regions. qRT-PCR primers were used to compare the expression of genes listed in **Table S5.**

2.4 Production of 7-MX and Culture Conditions

For experiments on plasmid expression, engineered EM42 colonies were placed in 5 mL of LB liquid medium supplemented with antibiotics (Depending on plasmid resistance, 50 mg/L Kanamycin and 25 mg/L chloramphenicol) were added for plasmid-based selection and incubated overnight at 30 °C, shaking at 250 rpm. The cells were harvested the following day by centrifugation at 4500 rpm for 5 min. The cell pellet was washed with 2XM9 solution and inoculated in 50 mL cultures of 2XM9 supplemented with 40 mM glycerol for 12 h at 30 °C, shaking at 250 rpm (respective antibiotic added). The cultures were again centrifuged, pelleted, and resuspended in 2XM9. The cultures incubated in glycerol were then added to 10 mL test cultures (in a 250 mL shake flask) with caffeine supplemented with 40 mM glycerol and antibiotics. Genome-integrated strains were cultured similarly without antibiotics unless resistant plasmids were added.

DOI: 10.1039/D5GC02883C

2.5 Growth assays

Pre-cultures of the strains were prepared by inoculating 5 mL M9 medium supplemented with 2 g/L glucose in 15 mL culture tubes and incubating shaking at 250 rpm, 30°C. At mid-log phase (OD_{600} 0.5-1.0), cells were harvested by centrifugation at 4500 rpm, and the cell pellets were washed twice and resuspended in M9 medium without a carbon source. These resuspended cells were used to inoculate microplate wells containing 200 µL of M9 medium supplemented with 40 mM glycerol and various concentrations of methylxanthines to OD_{600} 0.1. Microplates were then incubated at 30°C with maximum shaking, and growth was measured by reading the absorbance (OD_{600}) every 30 min using a Tecan Infinite M PLEX microplate reader. Growth rates were calculated according to the growth curve equation.

2.6 Bioreactor production of 7-MX

A Distek, Bione 1250 (Distek, Inc, NJ, USA) bioreactor unit was used for the bench-scale production of 7-MX. LJBJ600 was pre-cultured in LB broth overnight and the cells were pelleted by centrifugation at 4500 rpm for 10 min. The cell pellets were washed with 2XM9 and inoculated in 2 L of 2XM9 supplemented with 40 mM glycerol in the bioreactor to an initial cell density of (OD_{600} = 0.5). The cells were allowed to grow in 2XM9 media for 24 h (up to OD_{600} ~ 5) and 5 mM of caffeine was fed to the culture along with the addition of 40 mM glycerol at different intervals (~6 hours) to maintain glycerol in the culture. Samples were collected and analyzed by HPLC every 3 h intervals to monitor the caffeine and glycerol utilization **(Fig. 5A).** Caffeine was fed in batches of 5 mM when the caffeine concentration fell below 2 mM, as estimated by HPLC analysis of samples. The culture was maintained at 30 °C, 300 rpm, and dissolved oxygen (DO) at 100% for the entire culture period. The pH, temperature, and DO were monitored using the bioreactor control unit.

2.7 Extraction of 7-MX from culture broth

The culture was cooled down below 4 °C to precipitate 7-MX and the culture broth was centrifuged in 50 mL falcon tubes at 5000 rpm for 10 min to separate media, cells, and 7-MX, which was accumulated in the bottom **(Fig. 5B)**. The cells and the media were removed while the 7-MX pellets were pooled and dried in a vacuum evaporator (LABCONCO, Centrivap Concentrator, Marshall Scientific) at 60 °C for 6 h until a constant weight was reached. The powder was then weighed and stored in an air-tight container.

2.8 Detection and quantification of methylxanthines

Caffeine and related methylxanthines (7-MX, theobromine) identification and quantification were done using an HPLC system (Shimadzu LC-2050 series, Shimadzu Corporation) on a Shim-pack Velox C18 column (2.7µm, 4.6 × 100 mm). An isocratic elution program with mobile phase composition of Water: Methanol: Acetic acid in the ratio 85: 15: 0.5. The Mobile phase flow rate was maintained at 0.36 mL/min, and the column temperature was maintained at 40 °C. Identification of all the methylxanthines was based on the retention times using the photo Diode Array (PDA: 260 nm) detector coupled to the HPLC system. For quantification, matrix-matched calibration curves were prepared with authentic standards for each analyte in M9 solution (R^2 0.9981). The analytical method was partially validated according to the European Medicines Agency's guidelines on the validation of analytical procedures. To obtain 100% mass balance, 5% (v/v) 1N NaOH was added to the culture samples and prepared for HPLC analysis.

Glycerol was quantified in the same HPLC system in a Rezex ™ ROA-Organic acid H+ (8%) Column (300 mm, 7.8 mm, Phenomenex, USA) using an isocratic elution of 0.005 N H_2SO_4 in water. The column oven was maintained at 30 °C. Quantification was based on the RID detector coupled to the Shimadzu HPLC. A matrix-matched calibration curve was obtained in M9 minimal

media using standard glycerol at varying concentrations (R^2 0.9912). Calibration curves for all analytes are given in **Fig. S8.**

2.9 Analytical characterization of methylxanthines

Caffeine, 7-MX, and intermediate products (theobromine and paraxanthine) were quantified by HPLC coupled to PDA detector as described above. 7-MX produced in bacterial cultures was first confirmed by Liquid chromatography separation coupled to time-of-flight mass spectrometry (LC/TOF/MS) using a Waters Q-TOF operated in Electrospray ionization positive mode (ES^+).

Purity of the 7-MX was confirmed using HPLC and NMR. The NMR results were obtained from the NMR facility in the Department of Chemistry, Southern Illinois University. The spectrum was recorded in DMSO-d_6 with a Bruker DRX 500 NMR spectrometer at 299 K (JEOL, USA). The chemical shifts were relative to DMSO-d_6 using the standard δ notation in parts per million.

2.10 Enzymatic Analysis of *N*-Demethylase Genes: Investigating the Impact of 7-MX.

Recent studies implementing the N-demethylase genes have been bottlenecked by plateauing 7-MX production *in vivo*. Product inhibition by 7-MX represents a possible explanation for the observed reaction limit. To explore possible inhibitory effects, purified N-demethylase enzymes were obtained and combined with various concentrations of substrate and 7-MX. The corresponding reaction velocities were recorded according to Michaelis-Menten kinetics, and the inhibitory effect of 7-MX was verified.

Enzymes were generated by overnight culture in *E. coli* as described previously and purified by nickel affinity chromatography [24]. Product inhibition on purified NdmB + NdmD was characterized by the change in concentration of NADH as theobromine conversion occurred in the presence of an additional 7-MX. This rate was compared to reactions without additional 7-MX present. Absorbance at 340 nm was used to measure NADH concentration through the Beer-Lambert law as previously demonstrated [25]. Reactions were performed in 96-well plates in 200 µL triplicate with absorbance measurements by Agilent Biotech Synergy H1 Hybrid Microplate Reader every five seconds for ten minutes after the addition of NADH and mixing. Theobromine and 7-MX concentrations were varied, and the corresponding NADH consumption rates, proportional to the reaction velocity, were determined according to Michaelis-Menten kinetics **(Table S6).** HPLC data measuring 7-MX formation verified that the reaction rate corresponds to NADH consumption. Each 200 µL reaction contained 50 µM ferrous ammonium sulfate, 0.5 mM NADH, 0.15 mM NdmB, and 0.15 mM NdmD in 50 mM of a potassium phosphate buffer. Reactions containing 10, 50, 100, 200, 300, 400, and 500 µM theobromine substrate were each performed with 0, 0.1, 0.25, and 0.5 mM 7-MX present. The resulting kinetic data were fit to a double-reciprocal plot, also known as a Lineweaver-Burk plot, to determine corresponding Michaelis constants (K_m) and maximum reaction velocities (V_{max}). Production inhibition of 7-MX on purified NdmB + NdmD is uncompetitive based on the generated Lineweaver-Burk plot. The inhibition constant, K_i calculation is detailed in **Supplementary Materials and Methods 1.5.**

2.11 Procedure of Techno-Economic Analysis (TEA) and Life Cycle Analysis (LCA).

A preliminary life cycle analysis was performed on the 7-MX production process according to ISO 14040 and 14044, using a functional unit of 1 kg of purified 7-MX. The goal of the analysis was to evaluate hotspots of a cradle-to-gate production process and identify pathways to reduce impacts. All analysis was performed in OpenLCA 2.2.0 using the EcoInvent 3.7.1 database. Life cycle data for caffeine were taken from the literature; impacts of the co-production of caffeine and coffee beans were physically allocated [26]. The process was modeled based on bench-scale experimental data. Providers for flows were

modeled using the market for materials, ROW, GLO, or RER, as available, with the exception of high-voltage electricity, which was modeled using the production mix using the US-RFC grid. Life cycle impacts were calculated using the ReCiPe 2016 Midpoint (H) methodology [27].

Preliminary TEA was performed using Excel-based models to estimate the capital investment and operating costs of a 100-ton per year 7-MX production facility operating for 50 weeks per year to direct future research and major cost drivers. Benchtop experimental data was scaled to a 100-ton-per-year production facility using an Excel-based model. The process model consists of a culturing reactor, six 100-ton bioreactors, and the capacity to separate, extract, and purify the resulting product from cells, residual water, harmful byproducts, and salts, as shown in **Fig. 6A, Table S7)**. Each reactor operated as a batch process with a culturing time of 140 h; it was assumed that one set of separation, extraction, and purification equipment was needed for all six reactors. Solvents and process water were recycled on-site. Of note, the major constituents of each unit process were mass balanced, based on a detailed bioreactor study using precise analytical methods; minor constituents (e.g., residual micro- and macroelements in the bioreactor) were handled as waste and are assumed to be removed through the waste treatment process. Energy consumption was estimated for mixing, centrifugation, pumping, purification, and distillation. Capital costs were estimated using scaling relationships, and operating costs were estimated from pricing estimates and scaled up from bench-scale reactions [28, 29]. The E-factor and The Process Mass Intensity (PMI) were calculated considering the mass of all material inputs of the current study and comparing with the material inputs of the most recent biological method of production (Liu et al., 2024) and the Chinese patent granted in 2024 (CN202311696670.7B).[18] Calculations were performed in Microsoft Excel using input and output mass data from the bioreactor setup of biological methods.[30] In the E-factor calculation, cEF includes both solvents and water without recycling, while sEF exclude these components. The proposed process in this study aims to recycle the water and solvents. The PMI was calculated using the ACS Green Chemistry Institute PMI calculator.[31]

Supplementary information contains the additional materials and methods related to the study.

3.0 Results

3.1 *P. putida* EM42 as a novel host for caffeine *N*-demethylation

To enable caffeine metabolism in KT2440, we heterologously expressed the N-demethylation genes from CBB5 **(Fig. S10A).** The developed LJBJ110 strain expressing *ndmABCDE* can catabolize caffeine into xanthine through the intermediate compounds, theobromine, and 7-MX; this was confirmed with a systematic expression of pathway genes in plasmids **(Fig. S10B).** Next, we aimed to selectively convert caffeine to high-value 7-MX by constitutively expressing *ndmABD* using the *tac* promoter (strain LJBJ113) and tested the bioconversion capability with glucose as a co-substrate **(Fig. 1A)**. Notably, adding glucose only enabled a partial utilization of caffeine (only ~1.44 mM) in the M9 medium, suggesting the caffeine transporter might be a limiting factor **(Fig. 1B, C)**. Hence, we constitutively expressed putative caffeine permease (*cafP*) from CBB5 in LJBJ113 and developed LJBJ116 [15].

The strain, LJBJ116 did not show a significant improvement ($p > 0.05$) in caffeine utilization in the presence of glucose, suggesting that glucose might exert catabolic repression on caffeine utilization **(Fig. 1D)**. To this end, we tested alternative co-substrate glycerol and achieved 100% selective conversion of 5 mM caffeine to 7-MX (within 12 h) in a M9 medium supplemented with 40 mM of glycerol **(Fig. 1E)**. Of note, the same conversion was achieved with acetate as a

View Article Online
DOI: 10.1039/D5GC02883C

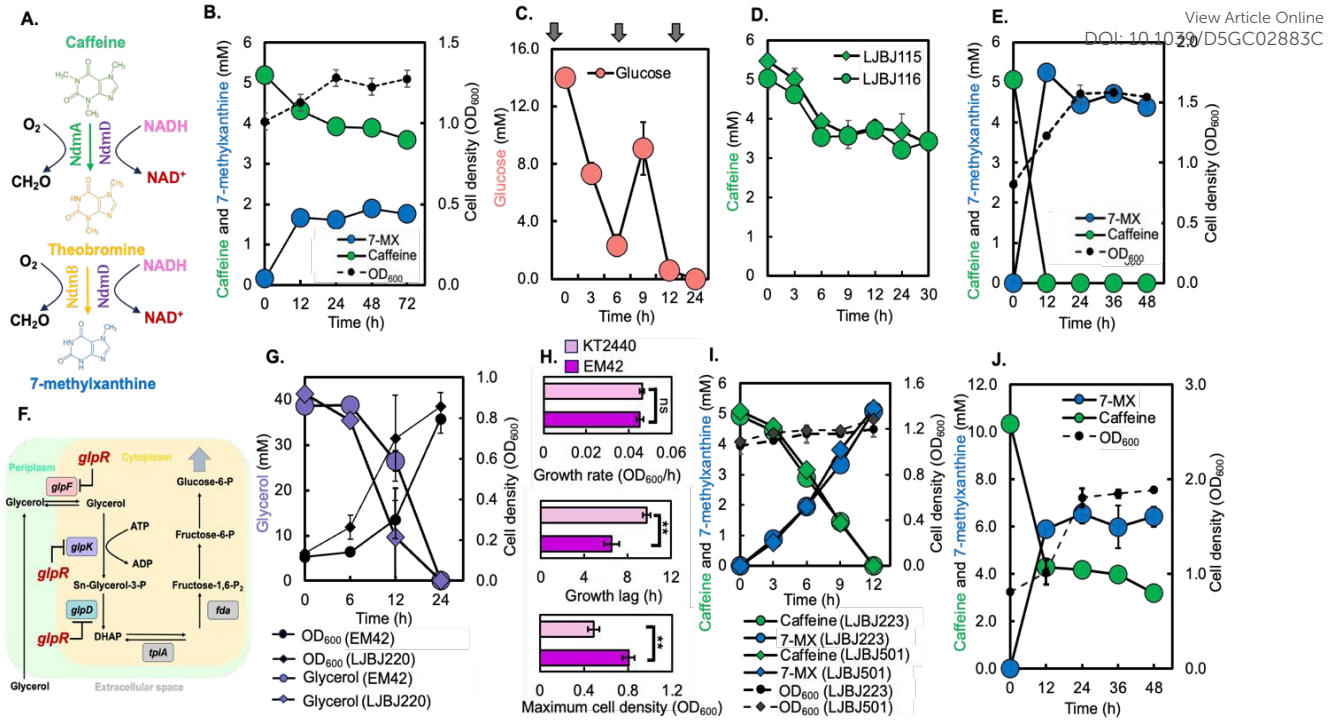

Fig. 1: Selective conversion of caffeine to 7-MX by heterologous expression of N-demethylase genes
(A), Schematic diagram of the N-demethylation pathway constructed in KT2440. **(B),** Caffeine utilization, 7-MX production, and **(C),** glucose utilization of LJBJ113 (KT2440::pBLT-2-P_{tac}-*ndmABD*$_{(kan)}$) strain in M9 medium supplemented with 11.11 mM (2 g/L) glucose (Gray arrow shows glucose feeding). **(D),** The effect of heterologous expression of *cafP* gene in KT2440 (LJBJ116, KT2440::pBLT2-P_{tac} *ndmABD + PBLT-2-*P_{tac} *cafP*$_{(chl)}$) compared to LJBJ115 (KT2440::pBLT-2-P_{tac} *ndmABD*$_{(kan)}$ *+ PBLT-2*$_{(chl)}$). **(E),** Caffeine utilization and 7-MX production of LJBJ113 (KT2440::pBLT-2-P_{tac}-*ndmABD*$_{(kan)}$*)* in M9 medium supplemented with 40 mM glycerol. **(F),** The schematic representation of glycerol metabolism in *P. putida.* **(G),** reduction of growth lag, and improved glycerol utilization achieved by genome deletion of *glpR* repressor in EM42 (LJBJ220, EM42::*ΔglpR*). **(H),** Comparison of growth rate, growth lag, and maximum cell density of KT2440$_{(wt)}$ and EM42$_{(wt)}$ with 5 mM of caffeine and 40 mM of glycerol in M9 media. **(I),** Caffeine utilization and 7-MX production of LJBJ223 (EM42::*glpRΔ*- pBLT-2-P_{tac}-*ndmABD*$_{(kan)}$) and P_{tac}-*ndmABD* genome integrated LJBJ501 (EM42::*glpRΔ*:P_{tac}-*ndmABD* + pBLT-2$_{(Kan)}$) in glycerol media with an initial caffeine concentration of 5 mM. **(J),** Caffeine utilization and 7-MX production of LJBJ500 (EM42::*glpR*Δ:P_{tac}-*ndmABD*) in glycerol media with an initial caffeine concentration of 10 mM. The results are expressed as means ± SEM (n=3). The level of statistical significance is indicated for differences between the two strains (**p <0.01).

co-substrate **(Fig. S10C)**. Since glycerol is a more industrially relevant, low-cost feedstock from biodiesel production, we decided to develop the process using glycerol as a co-substrate [32]. We speculated that the enhanced stress endurance of genome-reduced EM42 makes it an ideal chassis for 7-MX production [33]. Given that *P. putida* exhibits a significant (>22 h) growth lag in glycerol, we knocked out the transcriptional repressor, *glpR*, in EM42 **(Fig. 1F),** and the resulting LJBJ220 shortened the growth lag in glycerol to <6 h **(Fig. 1G),** and the lag phase can be eliminated by pre-culturing in M9-glycerol media **(Fig. S10D)** [34, 35]. Next, we overexpressed the *ndmABD* in LJBJ220 (plasmid-based) and compared the phenotype of developed LJBJ223 with its KT2440 equivalent strain, LJBJ221. We observed a shorter lag phase, high cell density, and increased 7-MX production rate in LJBJ223 relative to LJBJ221, where the final titer remained unchanged **(Fig. 1H, Fig. S10E, F)**. Based on this data, we decided to develop the EM42 platform further, and the copy of the synthetic *ndmABD* gene cassette was genome-integrated into EM42 genome using the *sacB* method to develop the strain LJBJ500 [36]. Notably, the shake flask test

View Article Online
DOI: 10.1039/D5GC02883C

revealed no significant difference (p >0.05) in yield, titer, and rate (YTR) of converting 5 mM caffeine to 7-MX between the *ndmADB* plasmid-bearing strain LJBJ223 and the genome-integrated strain LJBJ501 (LJBJ500 with empty plasmid) **(Fig. 1I)**. However, we found that LJBJ500 strain did not completely convert 10 mM

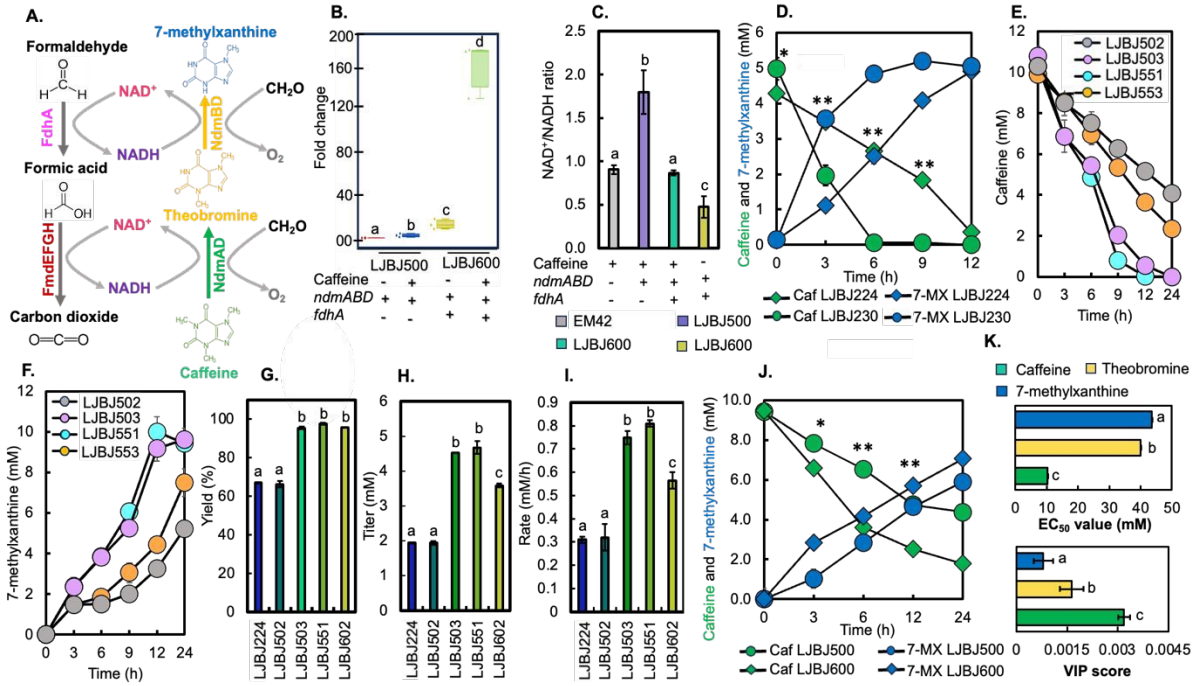

Fig. 2: Redox engineering of *P. putida* EM42 for efficient utilization of caffeine

(A), Schematic diagram of *N*-demethylation pathway and the formaldehyde detoxification pathway in EM42. NADH is oxidized during *N*-demethylation, whereas NAD^+ is reduced to NADH during formaldehyde oxidation to carbon dioxide. **(B),** Fold change of *fdhA* transcription of LJBJ500 (EM42::*glpR*Δ:P_{tac}*ndmABD*) and LJBJ600 (EM42::*glpR*Δ:P_{tac}*ndmABD*::P_{tac}-*fdhA*) strains in response to caffeine (10 mM) in glycerol media. **(C),** Comparison of NAD^+/NADH ratio of final production strain LJBJ600 (EM42::*glpR*Δ:P_{tac}*ndmABD*::P_{tac}-*fdhA*) and LJBJ500 strain (EM42::*glpR*Δ:P_{tac}*ndmABD)* with EM42 (*wild type*). **(D),** Comparison of caffeine utilization and 7-MX production of *fmdEFGH* and *fdhA* overexpressed strain LJBJ230 (EM42:: *glpR*Δ- pBLT-2-P_{tac}-*ndmABD* + pBLT-2-P_{lac}-*fdhA-fmdEFGH*$_{(chl)}$) and non-overexpressed LJBJ224 (EM42:: *glpR*Δ-pBLT-2-P_{tac}-*ndmABD* + pBLT-2$_{(Chl)}$) strain with 5 mM of initial caffeine concentration in M9 minimal salt medium supplemented with 40 mM of glycerol. **(E),** Comparison of caffeine utilization and **(F),** 7-MX production of the strains LJBJ502 (EM42::*glpR*Δ:P_{tac}*ndmABD* + pBLT2$_{(kan)}$ + pBLT-2$_{(chl)}$), LJBJ503 (EM42::*glpR*Δ:P_{tac}*ndmABD* + pBLT-2-P_{tac}-*fdhA* +pBLT-2 $_{(Kan)}$), LJBJ551 (EM42::*glpR*Δ:P_{tac}*ndmABD* + pBLT2-P_{tac}-*fdhA-fmdEFGH* + pBLT-2 $_{(Kan)}$), and LJBJ553 (EM42::*glpR*Δ:P_{tac}*ndmABD* + pBLT-2 $_{(Chl)}$-P_{lac} -*fmdEFGH* + pBLT-2 $_{(Kan)}$). **(G,H,I),** Comparison of YTR (yield, titer, and rate) of plasmid-bearing strains, LJBJ224 (EM42:: *glpR*Δ-pBLT-2-P_{tac}-*ndmABD* + pBLT-2$_{(Chl)}$), LJBJ503 (EM42::*glpR*Δ:P_{tac}*ndmABD* + pBLT-2-P_{tac}-*fdhA* +pBLT-2 $_{(Kan)}$) and LJBJ551 (EM42::*glpR*Δ:P_{tac}*ndmABD* + pBLT2-P_{tac}-*fdhA-fmdEFGH* + pBLT-2 $_{(Kan)}$) to its genome-integrated counterparts, LJBJ502 (EM42::*glpR*Δ:P_{tac}*ndmABD* + pBLT-2$_{(chl)}$ + pBLT-2$_{(kan)}$, LJBJ602 (EM42::*glpR*Δ:P_{tac}*ndmABD*::P_{tac}-*fdhA* + pBLT-2 $_{(Kanl)}$+ pBLT-2 $_{(Chl)}$) during the first 6 h of 10 mL cultures supplemented with 40 mM glycerol in M9 media. **(J),** Caffeine (Caf) utilization and 7-MX production of LJBJ500 (EM42::*glpR*Δ:P_{tac}*ndmABD)* and LJBJ600 (EM42::*glpR*Δ:P_{tac}*ndmABD*::P_{tac}-*fdhA)* with 10 mM of initial caffeine in M9 minimal salt media supplemented with 40 mM of glycerol. **(K),** Variable important parameter (VIP) score of caffeine, theobromine, and 7-MX. EC_{50} values of caffeine, theobromine, and 7-MX for EM42. The results are expressed as means ± SEM (n=2). The level of statistical significance is indicated for differences between the two strains (*p <0.05, **p <0.01). Bars labeled with different symbols (a, b, and c) indicate statistical significance in the differences (p < 0.05; one-way ANOVA followed by Tukey's post hoc honest significance difference test). Bars labeled with the same symbol indicate no statistically significant difference (p > 0.05). ANOVA: analysis of variance.

View Article Online
DOI: 10.1039/D5GC02883C

caffeine to 7-MX and demanded additional metabolic engineering to enhance the bioconversion (**Fig. 1J**).

3.2 Redox engineering of *P. putida* EM42 for efficient utilization of caffeine

Researchers leverage engineering redox cofactor balance to enhance the reaction rate of chemical reactions [37]. The N-demethylation reaction of caffeine to 7-MX relies on NADH and yields a toxic byproduct, formaldehyde, and NAD^+ [16, 38]. We speculated that the overexpression of *P. putida*'s native formaldehyde dehydrogenase (*fdhA*) and formate dehydrogenase (*fmdEFGH*) would enhance the redox coupling reactions while detoxifying the formaldehyde **(Fig. 2A)** [39]. Indeed, we found that the *fdhA* transcript level increased

by 4-fold in LJBJ500 strain (p < 0.05) in the presence of caffeine relative to the control, and the NAD^+/NADH ratio was ~2, indicating the redox imbalance **(Fig. 2B, C)**. Hence, we systematically evaluated the redox-balancing approach under caffeine to 7-MX conversion by plasmid-based expression of *fdhA* and *fmdEFGH,* monitoring the transcript levels of the genes, and measuring NAD^+/NADH ratio of the strains. The strain LJBJ230 expressing *fdhA* and the *fmdEFGH* gene cluster under a *lac* promoter utilized 5 mM of caffeine in 6 h with a 100% 7-MX yield **(Fig. 2D).** Indeed, the LJBJ230 remarkably enhanced (p < 0.05) the reaction rate relative to the control strain LJBJ224 and exhibited the near perfect redox cofactor balance ~1, in the presence of caffeine **(Fig. S11A)**. Next, we added the *fdhA* and *fmdEFGH* plasmid to LJBJ500 strain and tested the phenotype, which resulted in LJBJ551. Notably, the strain LJBJ551 enabled the complete conversion of 10 mM of initial caffeine to 7-MX at twice the higher rate compared to its control strain **(Fig. 2E, F)**. Since our qRT-PCR data didn't show significant expression of *fmdEFGH*, under caffeine condition in LJBJ500 strain **(Fig. S11B)**, we tested the effect of overexpressing *fdhA* alone in LJBJ500, using the developed LJBJ503. The results showed that overexpressing *fdhA* suffices to complete the conversion of 10 mM caffeine to 7-MX **(Fig 2E, F)**. We didn't observe a significant difference in YTR between the LJBJ503 and LJBJ551 **(Fig. 2G, H, I)**. Hence, we integrated an additional copy of *fdhA* under the *tac* promoter at the *glpRΔ* locus of LJBJ500 and developed the industrial-relevant antibiotic-free LJBJ600 strain. As expected *fdhA* expression significantly enhances the NADH pool (p < 0.05) in the cells under caffeine conversion relative to the absence of caffeine (**Fig. S11C**). Notably, this strain exhibits better redox balance, NAD^+/NADH ratio ~0.8 **(Fig. 2C, Fig. S11C, D),** significantly higher *fdhA* expression (160-fold relative to the control, p < 0.05) in the presence of caffeine **(Fig. 2B),** and significantly outperforms the LJBJ500 strain (p < 0.05) **(Fig. 2J)**. Collectively, these data suggest that the redox cofactor coupling in the LJBJ600 strain is enabled by the overexpression of *fdhA*, which converts NAD^+ generated through the demethylation reaction into NADH[40, 41]. However, unlike the plasmid-expressing LJBJ551 strain, LJBJ600 is unable to completely convert 10 mM of caffeine to 7-MX **(Fig. 2E, J)**. We evaluated the YTR of the LJBJ600 strain relative to the plasmid-bearing strains, the rate and titer at 6 h of LJBJ602 (LJBJ600 with empty plasmid) were ~20 % lower (p <0.05) compared to its plasmid-bearing counterpart LJBJ503 **(Fig. 2G, H, I)**. Of note, we added an extra *lac* promoter-driven *fmdEFGH* copy to the genome of LJBJ600 (LJBJ700) to determine if enhanced formate dehydrogenase activity could restore performance. However, the developed LJBJ700 did not significantly improve the YTR parameters (p < 0.05). **(Fig. S11E, F)**.

Methylxanthines pose chemical toxicity on host bacterial strains, and understanding the chemical toxicity effect of substrates (e.g., caffeine) and products (e.g., 7-MX) on *P. putida* helped us to develop the process to alleviate the toxicity [42]. Hence, we comprehensively analyzed the singular and combinatorial toxicity of the compounds**.** The data revealed that caffeine has a low EC_{50} value of 10±0.8 mM relative to the other tested compounds **(Fig. 2K)**. Also, caffeine and 7-MX have a combinatorial effect on the growth of

View Article Online
DOI: 10.1039/D5GC02883C

EM42, **(Fig. 2K, Fig. S11G)**. The VIP score unveiled that caffeine contributed more to the combinatorial inhibitory effect. Hence, understanding the molecular targets of caffeine in EM42, particularly LJBJ500 under caffeine utilization, is essential for further developing the strain to produce high-value methylxanthine.

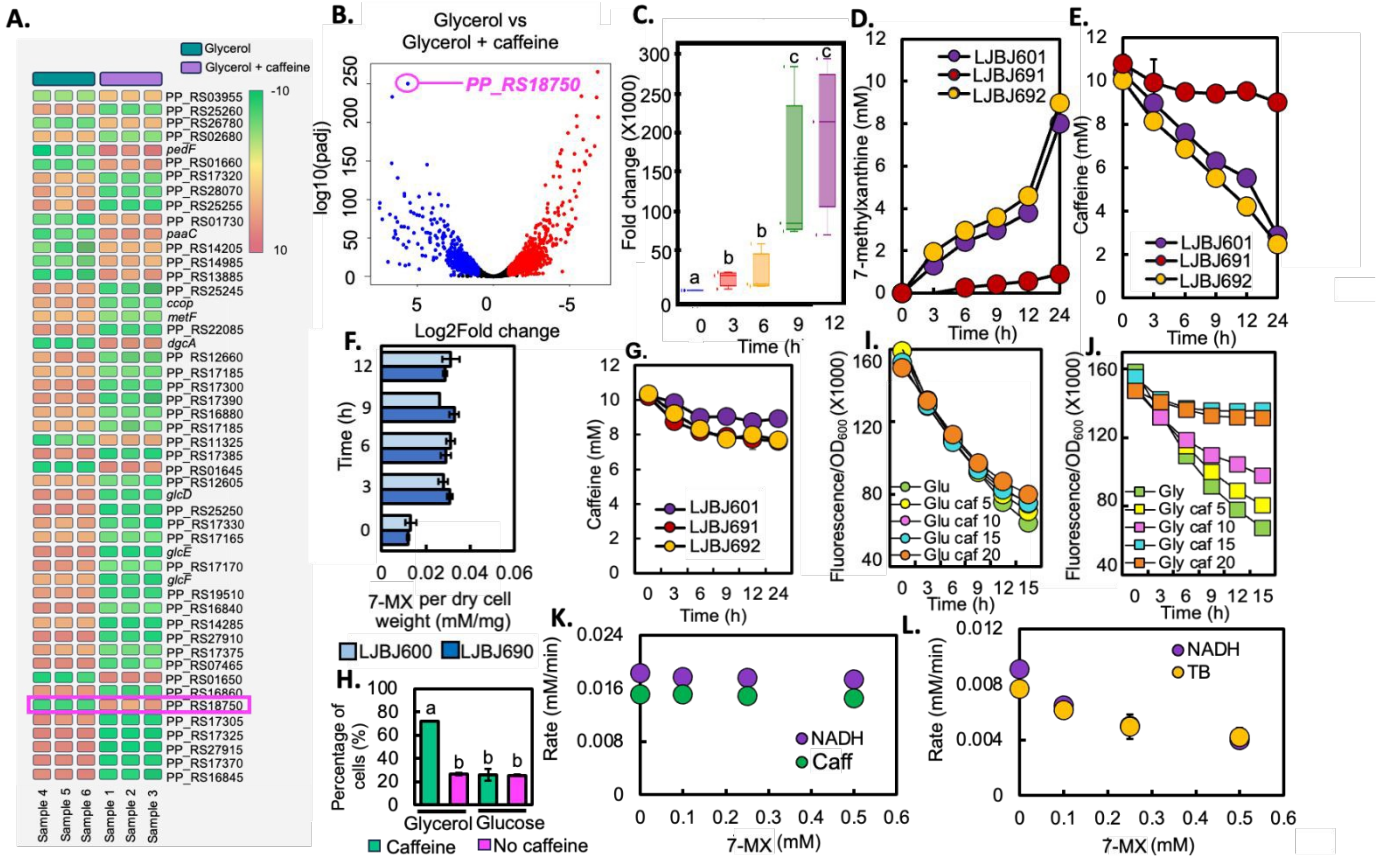

Fig.3: Characterization of the novel caffeine transporter *PP_RS18750* and the feedback inhibition of 7-MX on N-demethylase enzymes.

(A), Heat map of the genes with highest adjusted *p*-values in LJBJ500 (EM42::*glpR*Δ:P_{tac}*ndmABD*) treated with and without caffeine in glycerol media. **(B),** Volcanic plot showing the differential expression of genes with and without caffeine in glycerol media. *PP_RS18750* encodes for DMT family transporter is labelled on the volcanic plot. **(C),** Expression profile of *PP_RS18750* with the time of LJBJ500 (EM42::*glpR*Δ:P_{tac}*ndmABD*) in glycerol-caffeine with respect to glycerol. **(D,E),** 7-MX production and caffeine utilization were drastically reduced in LJBJ691 (EM42::*glpR*Δ:P_{tac}*ndmABD*::P_{tac}-*fdhA:PP_RS18750*Δ + pBLT-$2_{(kan)}$), and the caffeine utilization and 7-MX production were restored once *PP_RS18750* was expressed in a plasmid in *PP_RS18750* deleted strain, LJBJ692 (EM42::*glpR*Δ:P_{tac}*ndmABD*::P_{tac}-*fdhA:PP_RS18750*Δ + pBLT-2-P_{tac}-*PP_RS18750*$_{(kan)}$). **(F),** 7-MX (mM) retained per mg of dry cells of LJBJ600 (EM42::*glpR*Δ:P_{tac}*ndmABD*::P_{tac}-*fdhA)* and LJBJ690 (EM42::*glpR*Δ:P_{tac}*ndmABD*::P_{tac}-*fdhA:PP_RS18750*Δ). **(G),** Caffeine utilization of LJBJ691 (EM42::*glpR*Δ:P_{tac}*ndmABD*::P_{tac}-*fdhA:PP_RS18750*Δ + pBLT-$2_{(kan)}$), LJBJ601 (EM42::*glpR*Δ:P_{tac}*ndmABD*::P_{tac}-*fdhA* + pBLT-$2_{(Kan)}$) and, LJBJ692 (EM42::*glpR*Δ:P_{tac}*ndmABD*::P_{tac}-*fdhA:PP_RS18750*Δ + pBLT-2-P_{tac}-*PP_RS18750*$_{(kan)}$) in glucose media. **(H),** Percentage of cells expressing GFP as detected by flow cytometry. A higher (∽72%) cells were expressing GFP in glycerol + caffeine condition compared to glycerol alone and glucose condition with and without caffeine. **(I, J),** Fluorescence normalized to cell density in glucose (Glu) and glycerol (Gly) containing 10 mM of caffeine (Caf). **(K),** Caffeine (Caff) degradation reaction with N-demethylase NdmA and NdmD with 0.5mM of caffeine and various concentrations of 7-MX as substrate. **(L),** NADH consumption rate and the Theobromine [TB] degradation rate under the presence of extra 7-MX as a part of the substrate for the N-demethylase NdmB and NdmD.

3.3 Identification of novel caffeine transporter in *P. putida* EM42.

To understand the glycerol-enabled caffeine biotransformation to 7-MX and the inhibitory effect of caffeine on EM42, we deployed an RNA-seq study with the samples obtained with M9 medium containing glycerol with or without caffeine at EC_{50} concentration (10 mM). Our analysis identified 251 upregulated and 345 downregulated genes (log2FoldChange, $p < 0.01$) when glycerol and caffeine were present together, relative to conditions with glycerol alone **(Fig. 3A, B).** Among the upregulated genes, we noted enrichment in biological processes such as electron transport and transcription regulation. Conversely, the molecular functions related to signalling receptor activity and transferase activity were found to be decreased in the presence of caffeine, as indicated in the Database for Annotation, Visualization, and Integrated Discovery (DAVID) **(ESI 4.0, 5.0).** A additionally, the complete analysis report and the functional categories can be found in the supplementary data **(ESI 4.0-6.0).** We observed that caffeine utilization ceased in the presence of glucose but continued with glycerol **(Fig. 1B-E**). This led us to speculate that catabolic repression of caffeine transporters may play a significant role in enabling caffeine utilization under glycerol conditions in EM42. Therefore, we specifically aimed to identify potential transporters through RNA-seq data that facilitate caffeine utilization in glycerol media. Our analysis revealed that *PP_RS18750* **(Fig. 3A, B),** a putative member of the drug/metabolites family of transporters (DMT), was one of the most highly upregulated genes in the caffeine and glycerol condition (log2FoldChange of 5.61). In contrast, it was significantly downregulated in the glucose-caffeine condition (log2FoldChange of -7.03) **(Fig. S12A, B)**. Homology modelling using AlphaFold and phylogenetic analysis indicates that this transporter is closely related to *P. putida*'s transporter, which contains the DMT domain, and to the plant DMTs that transport methylxanthines [43] **(Fig. S12C, Fig. S13)**. Notably, homology modelling revealed that *PP_RS18750* was aligned with CafP with a moderate score **(S14).** This is reflected in the phylogenetic tree, where CafP is shown to be distantly related to PP_RS18750 (**Fig. S13**). We reconfirmed the expression of *PP_RS18750* in the glycerol-caffeine medium compared to the glycerol medium using qRT-PCR **(Fig. 3C)**.

Next, we knocked out *PP_RS18750* in the LJ600 strain. The developed LJBJ690 was unable to utilize caffeine. The strain that contained a plasmid-based constitutive overexpression of *PP_RS18750* (LJBJ692) restored the phenotype of LJBJ691 (LJBJ690 with empty plasmid), confirming its involvement in caffeine uptake **(Fig. 3D, E)**. We found that the LJBJ690 strain did not accumulate 7-MX at a level comparable to LJBJ600, which ruled out its function as an exporter, unlike the majority of the DMT family proteins **(Fig. 3F)** [44, 45]. Furthermore, we tested LJBJ690 with other methylated xanthines, including theobromine and 7-MX **(Fig. S12D, E)**. Notably, the results revealed a novel role for *PP_RS18750* as a methylxanthine transporter **(Fig. S12E)**. We overexpressed *PP_RS18750* in LJBJ600 and tested the strain's ability to utilize caffeine in a glucose medium; however, the strain was unable to metabolize caffeine **(Fig. 3G)**. To track the transporter, we tagged sfGFP to the C-terminus of *PP_RS18750* under the constitutive *tac* promoter in LJBJ693 **(Fig. 3H, Fig. S12F, S15)** and functionally expressed it in LJBJ690 (LJBJ693) **(Fig. 3H, Fig. S12H)**. The microscopic images and FACS data confirmed a weak GFP signal in glucose media treated with caffeine for 3 hours despite the expression of *PP_RS18750*_GFP. Indeed, qRT-PCR data indicated that the strain maintained a constant transcript level of *PP_RS18750* **(Fig. S12G)**. Notably, periodic monitoring of the GFP intensity revealed a decreasing trend for *PP_RS18750*_GFP under glucose and glycerol conditions, while the intensity was sustained in caffeine-containing glycerol media in a concentration-dependent manner **(Fig. 3I, J)**. For instance, after 12 hours, the GFP fluorescence

View Article Online
DOI: 10.1039/D5GC02883C

intensity of *PP_RS18750* was significantly higher ($p < 0.05$) with different caffeine concentrations (up to 15 mM) **(Fig. S16)**. These findings suggest that *PP_RS18750* might tightly regulate at the post-transcriptional and/or translational levels, warranting further investigation into the regulatory mechanisms in future studies. Feedback inhibition of enzymes by their products can lead to a titer gap [46]. At a higher caffeine concentration of 10 mM, the LJBJ600 strain culture samples showed a slight accumulation of theobromine (~0.3 mM). Of note, at this concentration, 7-MX had a minimal effect on cell growth inhibition. This observation led us to hypothesize that feedback inhibition by 7-MX may occur within the strain. To investigate this further, we examined the feedback inhibitory effect of 7-MX on the N-demethylase enzymes through biochemical assays. The data indicated, conversion of caffeine to theobromine by NdmA was not affected by 7-MX **(Fig. 3K)**. In contrast, the activity of the enzyme NdmB decreased significantly ($p < 0.05$) with increasing concentrations of 7-MX, showing around a 50% reduction compared to the control group at 0.5 mM 7-MX **(Fig. 3L, Fig. S12I, J, K)**. This data revealed the uncompetitive inhibitory effect of 7-MX on NdmB, with a K_i value of 553±40 µM **(Table S7).** Notably, it is evident that the intracellular concentration of 7-MX remained below 0.04 mM/g of cell dry weight, well below the K_i **(Fig. 3F)**, indicating minimal feedback inhibition (less

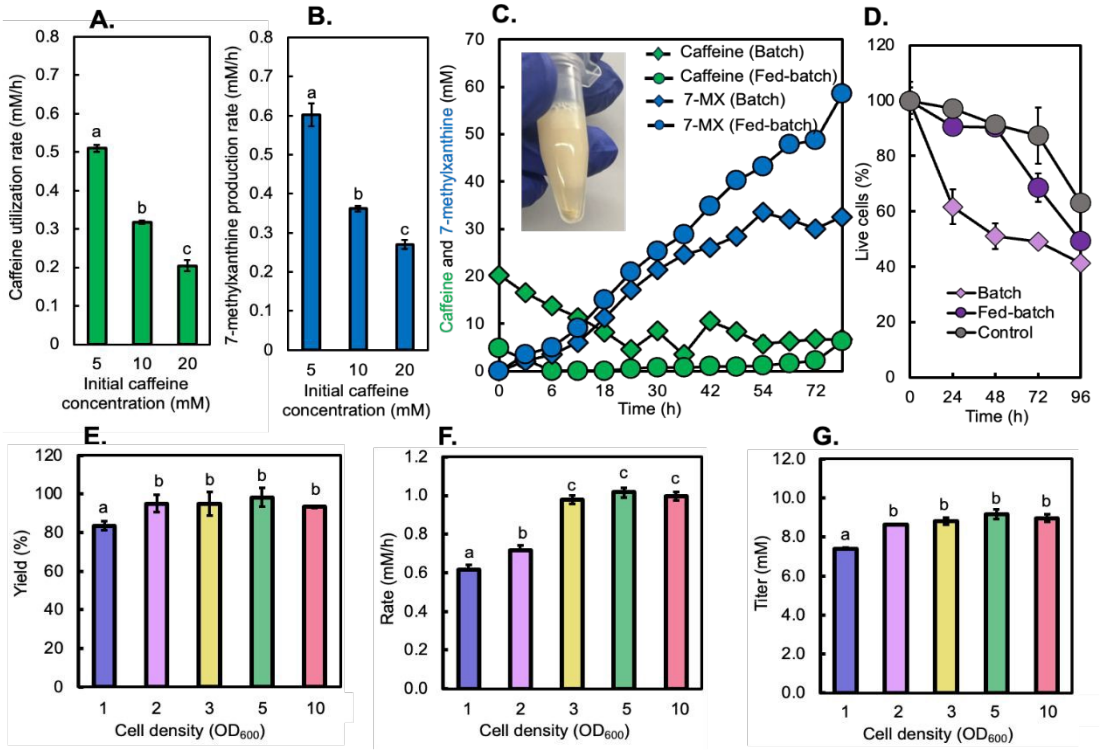

Fig.4: A. Optimization of culture technique and culture parameters.

(A), Caffeine utilization rate and **(B),** 7-MX production rate with the caffeine concentration added at the start of the culture. **(C),** Caffeine utilization, 7-MX production over time in batch culture and fed-batch culture techniques. The Inset image shows the precipitation of 7-MX in the bottom due to the suboptimal solubility of 7-MX in M9 media. **(D),** Live cells percentage of batch culture and fed-batch cultures. Comparison of yield **(E),** rate **(F),** and titer **(G),** with increasing initial cell density measured as OD_{600}. Bars labeled with different symbols (a, b, and c) indicate statistical significance in the differences in growth rate between those strains ($p < 0.05$; one-way ANOVA followed by Tukey's post hoc honest significance difference test). Bars labeled with the same symbol indicate no statistically significant difference ($p > 0.05$). ANOVA: analysis of variance. The results are expressed as means ± SEM (n=3). The level of statistical significance is indicated for differences between the two strains (**p <0.05).

View Article Online
DOI: 10.1039/D5GC02883C

than 10%), suggesting that the feedback inhibition of 7-MX on NdmB in the LJBJ600 strain presents only a minor bottleneck for achieving a high titer of 7-MX. Collectively, these data suggest that process-level optimization, such as fed-batch growth, can be used to mitigate the toxicity effect of caffeine and product 7-MX and enhance the final titer.

3.4 Batch-culture technique to overcome substrate toxicity.

Batch culturing of LJBJ600 at a high initial caffeine concentration of ≥ 10 mM resulted in a significant reduction in YTR parameters and growth **(Fig. 4A, B, C).** A live/dead cell assay indicated that only 60% of the cells were viable after 24 hours, and this viability continued to decline over time **(Fig. 4D).** To address substrate-level toxicity, we tested a fed-batch process using 5 mM caffeine **(Fig. 4B, S17A, B).** The data demonstrated that LJBJ600 can efficiently utilize caffeine at this concentration, administered at 6 h intervals. As a result, we achieved a maximum 7-MX titer, 58 ± 0.16 mM at 96 h, yielding the highest titer recorded to date for a bacterial monoculture system. The live/dead cell assay indicated a significant improvement in live cell population ($p < 0.05$), which sharply declined after 48 h of incubation and ultimately halted the reaction at 96 hours **(Fig. 4D).** Given that an increased initial cell density helps manage the initial chemical toxicity in microbial biocatalysts, we assessed the YTR parameters for conversion of caffeine to 7-MX using different cell densities from LJBJ600. We found that an initial cell density of $OD_{600} > 3$ significantly enhanced the YTR parameters compared to $OD_{600} = 1$ **(Fig. 4E, F, G)**. Based on these results, we decided to develop larger headspace in shake flasks to achieve efficient and complete conversion of caffeine to 7-MX **(Fig. S17C, D).** Liu and co-workers noted that a higher oxygen requirement is necessary for N-demethylation and alleviation of formaldehyde toxicity[38]. We next aimed to develop the fed-batch process using a benchtop bioreactor to scale up and obtain the process parameters to run techno-economic (TEA) and life cycle analysis (LCA).

3.5 Scaling up to bioreactor production, purification, TEA, and LCA

We adopted a fed-batch process in a 5-L bioreactor with LJBJ600 and added 5 mM of caffeine periodically after the optical density reached a value of 5 or greater (**Fig. 5A**). We continued to supplement caffeine and glycerol until the viable cell count dropped below 10%. As a result, we successfully converted caffeine to 7-MX with a yield of 100% (mol/mol), achieving a titer of 9.22 ± 0.42 g/L (56 ± 1.66 mM) and a rate of 0.098 ± 0.004 g/L/h. This marks the highest titer of microbially produced 7-MX reported to date, with a total of 3 L of culture in M9 media supplemented with glycerol **(Fig. 5A, B)**. Next, we explored cost-effective separation techniques besides the commonly implemented prep-scale HPLC for extracting methylxanthines from the culture broth [13, 14, 19, 47]. Indeed, low-temperature storage (~12 h, 4 °C) precipitated 7-MX as clumps in the bottom of the glass bottles containing bioreactor culture broth (**Fig. 5C**). Centrifugation enabled the separation of liquid media and cells from the 7-MX pellet, which was distinguishable (**Fig. 5D**). The obtained pale yellowish powder dried through the rotary evaporator represents 78.04 ± 4.1% product recovery (**Fig. 5E**), and rest of the product (i.e., cell intact 7-MX) can be recovered through column separation[13]. We used column and solvent-based endotoxin removal and reduced the endotoxin concentration to 0.52 ± 0.003 EU/mL for making the pharmaceutical grade 7-MX (**Fig. S9**). Chemical characterization via LC-MS total ion current (TIC) profiling, in comparison with a commercial 7-MX standard, confirmed purity of >98% (**Fig. 5F**). Further analyses using TOF-MS/MS (**Fig. S17E**), 1H-NMR, and 13C-NMR spectra confirmed the structure and purity of the biochemically produced 7-MX (**Fig. 5G, Fig. S18**).

View Article Online
DOI: 10.1039/D5GC02883C

We performed preliminary LCA and TEA to estimate the costs and environmental impacts of the 7-MX production process. When fixed and variable costs are accounted for a 100-ton-per-year facility, the minimum selling price (MSP) of the 7-MX is $328/kg **(Fig. 6B, Table S8, S9)**. The production of 1 kg of 7-MX results in 35.2 kg CO_2 equivalent, and over 50% of the Global Warming Potential (GWP) impacts are associated with high energy usage in heating and cooling water used to maintain the temperature in the bioreactor and subsequent separation step **(Fig. 6C, Table S10).** The detailed environmental impact assessment of the LCA is available in **Table S10**. Caffeine was another large contributor to GWP, primarily due to commercial extraction using supercritical CO_2[26]. The solubility of caffeine in water was the single most critical factor in the facility design and the environmental impacts. Continuous dosing of caffeine into the reactor is

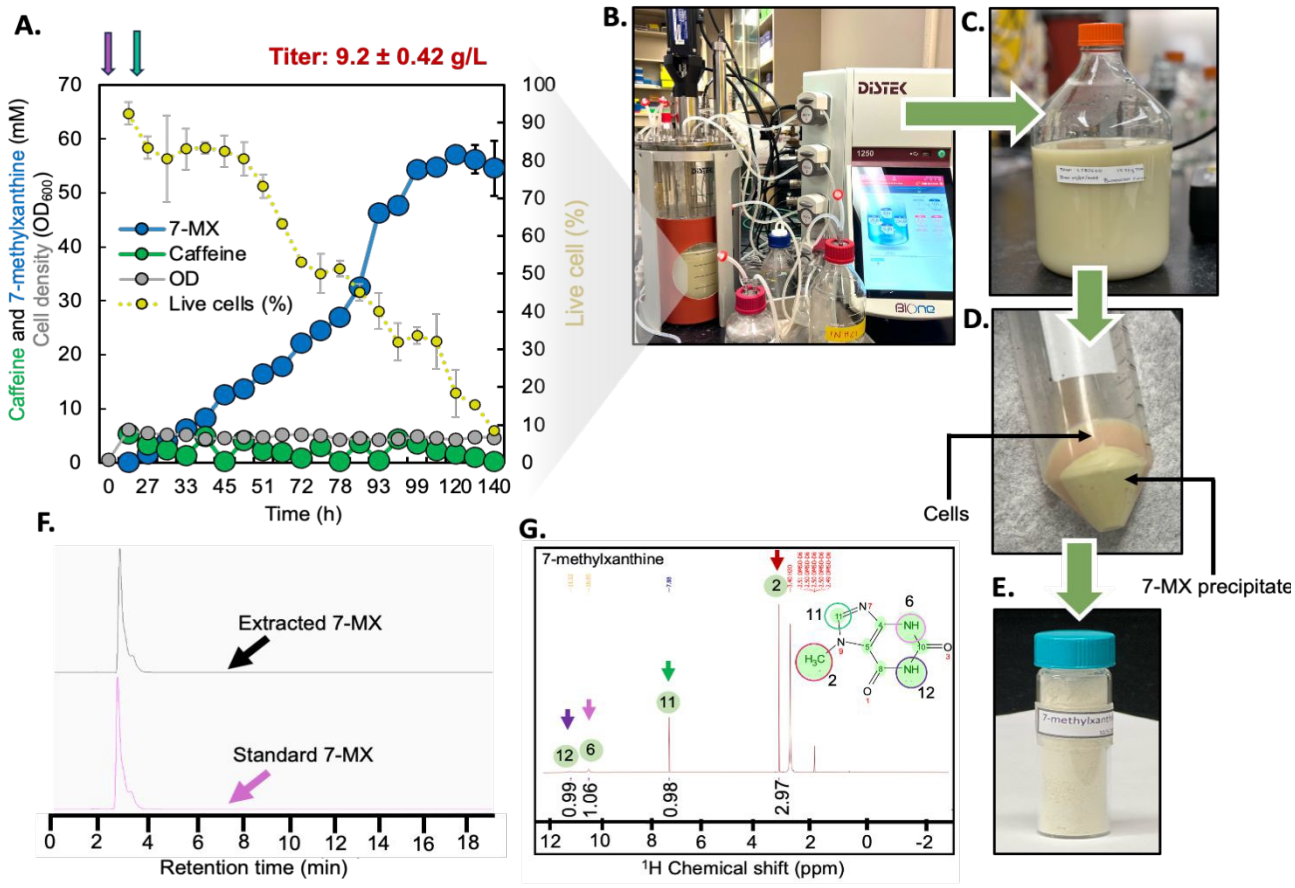

Fig.5: Bioreactor production and extraction of 7-methylxanthine

(A), Bioreactor production of 7-MX by batch-feeding of caffeine (5 mM). Glycerol was fed at 24 h intervals starting from t=0 (pink arrow) and caffeine was fed starting from 24 h (green arrow) when the cell density reached OD_{600} of 5. Live cell % was monitored throughout the culture duration. Bioreactor set-up used in the culture process and culture broth upon termination of the bioreactor. **(B),** Distek 1250 Bench-scale bioreactor used for production of 7-MX. **(C),** Fermented culture broth before cold storage **(D),**7-MX precipitated in the bottom of the falcon tube when stored at 4 °C and centrifuged at 5000 rpm for 10 min. **(E),** 7-MX powder after separation and drying. **(F),** Comparison of the chromatograms of 7-MX commercial standard (98% purity, pink arrow) and extracted 7-MX powder (>98% purity, black arrow), appears as a single peak at retention time 3.4 min. **(G),** The NMR spectrum of extracted 7-MX was recorded in DMSO-d_6 with a Bruker DRX 500 NMR spectrometer at 299 K, ^{1}H NMR (500 MHz, DMSO-D_6) δ 11.52 (δ, 1H), 10.85 (δ, 1H), 7.88 (δ, 1H), 3.81 (δ, 3H). The hydrogen atom corresponding to the peak is labeled and circled in the same color. The X-axis denotes 1H Chemical shift (ppm). The results are expressed as means ± SEM (n=3).

View Article Online
DOI: 10.1039/D5GC02883C

expected to reduce the total volume of water needed, significantly lowering energy and purification costs and reducing capital expenditures. We conducted preliminary experiments to test caffeine powder dosing in shake flasks and assessed the preliminary process compatibility **(Fig. S19).** Of note, unlike the plasmid-bearing strain, the genome-integrated LJBJ600 is highly stable, and can be stored long-term through cryopreservation and used for preculture preparation. Since the process does not recirculate used cells, mutations occurring during bioreactor culturing won't affect the overall process. Our strain (YTR) has shown consistent performance across generations, with shake flask and bioreactor studies. Thus, the TEA does not include genetic instability costs**.** Future studies will evaluate pilot-scale processes to ensure improved efficiency and cost-effectiveness. Notably, the processes described has an E-factor (sEF) value of ~63%, which is lower than that of a previously published biological process (**Fig. 6C, Table S11**). Additionally, it demonstrates an ~81% reduction in E-factor (sEF) compared to a recently published patent for the chemical synthesis of 7-MX (**Fig. 6C, Table S11)**. Also, the current method achieves ~14% reduction in total PMI with PMI Substrates and Reagents being ~166% lower than the previous biological process (**Table S11)**. In comparison to the chemical process, the new approach demonstrates ~212% reduction in PMI Substrates and Reagents, and ~500% reduction in PMI for solvents (**Table S11**). It is important to note that the chemical process uses toxic chemicals and solvents.

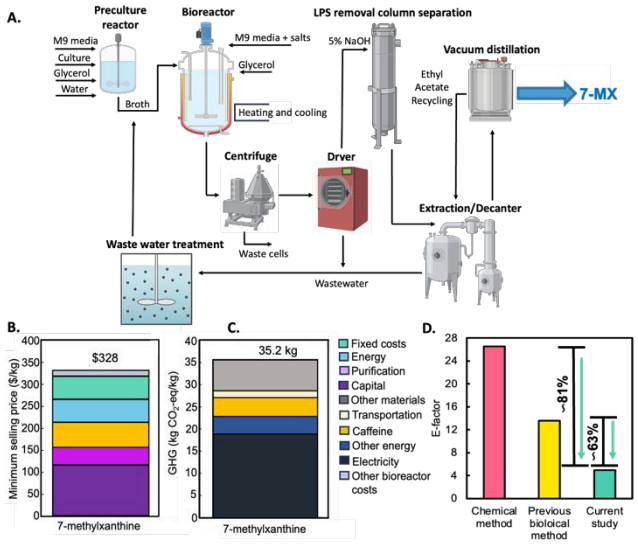

Fig.6. Schematic diagram of the proposed large-scale production process and the TEA and LCA analysis.

(A), Capital expenditures for the equipment of a 100-ton-per-year facility were estimated to cost $34,600,000, using a Lang factor of 4.74 results in an Inside Battery Limit (ISBL) of $164,004,000. Outside Battery Limit (OBSL) costs were assumed to be 40% of ISBL costs ($65,601,600), resulting in an estimated capital expenditure of $229,605,600. When fixed and variable costs are accounted for, the minimum selling price of the 7-methylxanthine is $328/kg. **(B),** The major costs associated with the production process and the respective cost components. **(C),** Life cycle analysis (LCA) depicts the greenhouse gas emission (GHG) of the associated inputs of the production process. **(D),** E-factor (sEF: without water and solvent) comparison of the current study and the most recent study on the chemical (CN202311696670.7B) and biological production of 7-MX (Liu *et al*.,2024).

In addition, bio-based production processes can decrease human and ecological toxicity **(Table S12,13).** Additionally, the toxicity of precursors can influence manufacturing practices and guidelines. To investigate this aspect in the production of methylated xanthines, we used the Environmental Protection Agency (EPA) Toxicity Estimation Software Tool (TEST) to compare the chemical synthesis process with the developed biological synthesis process of 7-MX, considering various human and environmental factors. The computational tool predictions suggest that the compounds used for the biological synthesis and purification of 7-MX are not mutagenic and have a notably higher oral rat, median lethal dose, LD50 (e.g., > 5000 mg/Kg for the biological vs <3500 mg/kg for the chemical process) and low development toxicity value (< 0.6 for the only positive compound, ethyl acetate) than those employed in chemical synthesis **(Table S12, 13).**

4.0 Discussion

A two-tier system for combating chemical toxicity, comprising detoxification and protection of macromolecules, has enhanced the robustness of EM42 strain and can help overcome the toxicity of methylxanthines, ultimately leading to improved production titers [22, 48, 49]. Specifically, caffeine and its N-demethylated products, 7-MX, exhibit antibacterial activity against microbial host strains **(Fig. S17F-J)**[38]. Our RNA-seq data is a rich source to identify potential molecular targets of caffeine-related DNA damage response and protein quality control under caffeine stress, aiding the rational engineering of LJBJ600. **(ESI 4.0, 5.0)**. In fact, researchers have implemented adaptive laboratory evolution (ALE) to fine-tune the engineered pathways and enhance production parameters [50-53]. We have also been evolving LJBJ600 to further improve the chemical robustness of the strain in response to caffeine (achieved 3X tolerance to caffeine, data not shown) and undertaking multi-omics studies to identify the key regulators and gene targets. Based on the study, we will direct our work to enhance cell viability (**Fig. 4D**) and optimize the production parameters for 7-MX in LJBJ600, addressing the toxicity of both caffeine and 7-MX.

Researchers can utilize a cell-free system to produce methylated xanthines by coupling the N-demethylation reaction with redox regeneration reactions [54]. Studies indicate that the conversion of theobromine to 7-MX is a rate-limiting step in producing 7-MX[24]. Our biochemical analysis revealed that the feedback inhibition of NdmB is a key factor contributing to the observed phenotype **(Fig. 3L)** and can pose a significant challenge to both cell-free and cell-intact production systems. The evolution of the enzyme through an in silico-guided approach and/or applying selection pressure can be employed to eliminate product inhibition and enhance the reaction rate [55]. Also, balancing the reaction rates of both demethylation and redox reactions can enhance the overall reaction kinetics of caffeine to 7-MX conversion [37]. Indeed, our data reveals that the addition of multi-copy plasmid *fdhA* and *fmdEFGH* improved the reaction rate of LJBJ600 **(Fig. S11H).** Implementing synthetic redox balance strategies based on multi-omics, including comprehensive fluxomics, can be leveraged to enhance LJBJ600 YTR parameters further [56]. LysR and Crc proteins are involved in metabolic pathways in *P. putida* [57-59]. For instance, Crc is bound to the 5′ end of *benR* mRNA and reduces the benzoate uptake at the translational level. We found the key transporter, *PP_RS17850*, which enables the trafficking of caffeine, is regulated transcriptionally, post-transcriptionally, and translationally based on the carbon source and concentration of caffeine **(Fig. 3J, K).**

Using a comprehensive RNA-seq and reverse engineering approach, we discovered a conserved membrane protein of unknown function, *PP_RS18750*, which facilitates the trafficking of methylated xanthine(s) and enables their conversion to desired product(s) **(Fig. 3A-H)**. This finding provides new molecular-level insights into the mechanisms behind biological processes that allow for the utilization of the low-cost co-substrate glycerol in the production of the compound. Our RNA-seq data shows high expression of LysR family transcriptional regulator, *PP_RS18745*, which is located upstream of *PP_RS18750* (~4-fold upregulation in the caffeine-glycerol condition relative to the caffeine-glucose); further investigation of this regulator may decode the regulatory mechanism of *PP_RS18750* **(Table S6.2).** Systematic characterization is necessary to decode the regulation cascade in both transcriptional and post-transcriptional regulation of the novel-identified methylated xanthine transporter, *PP_RS17850*. The investigation of caffeine intake and the crosstalk of caffeine in different carbon sources is a very interesting topic that goes beyond the optimization of the methylated xanthine synthesis pathway. Recently, researchers identified a metabolic link between coffee consumption and the dynamics of the abundance of specific gut microorganisms across

View Article Online
DOI: 10.1039/D5GC02883C

different human populations[60]. The abundance of *Lawsonibacter asaccharolyticus* enables the utilization of caffeine. Our study provides new insight into finding the potential transporter(s) and caffeine-mediated molecular regulation(s) in those communities and emphasizes the need for future comprehensive biochemical investigations.

Using waste caffeine streams, such as spent coffee and tea, might further enhance the product's economic benefits. Indeed, we have used the thermochemically treated waste tea hydrolysate and enabled the conversion of caffeine to 7-MX with 100% yield **(Fig. S20)** [61]. However, the heterogeneity of the substrate caused an issue with recovering the products at high purity; adopting microbial funnel techniques, a priory separation of caffeine in waste coffee via ionic or supercritical CO_2 extraction, or developing affinity column-based or *in situ* membrane-based separation techniques could be adapted for use of those substrate streams, and we are currently investigating those approaches [26, 62]. Indeed, developing a process for *in situ* product extraction may help reduce the primary cost factors while maintaining cell survival by minimizing the chemical toxicity of products.

TEA confirmed the developed process enables >1500X value improvement to caffeine based on MSP and the current market price of 7-MX **(Table S14)**. The proposed process has a remarkably lower E-factor and PMI values than other biological and chemical synthesis methods and does not utilize hazardous chemicals, demonstrating the green synthesis of 7-MX. Reducing water and solvents is crucial for further improving green metrics. Indeed, we present a preliminary techno-economic and life cycle analysis that aims to demonstrate the impact of green processes on synthesizing 7-MX. This work will serve as a foundation for future TEA and LCA-driven process optimization (e.g., reducing water usage and sourcing renewable energy) and facilitate the comparison of technologies for commercial manufacturers interested in this field.

Our developed process can be adapted to produce other methylated xanthines by rearranging or mutating N-demethylated enzymes [19, 42, 47]. For example, knocking out the enzyme NdmB from LJBJ600 allows for a complete conversion of caffeine to theobromine, while eliminating NdmA converts theophylline to 3-MX in an M9-glycerol medium (data not shown). We are working on expanding the range of products and enhancing YTR by further engineering the base strain LJBJ600.

5.0 Conclusions

In this study, we developed the industrially relevant microbial biocatalyst, a robust monoculture that can achieve the highest titer of 9.2 ± 0.42 g/L, 7-MX to date with process optimization in M9 media supplemented with glycerol as co-substrate **(Fig. 5A)**. It remarkably outperformed existing methods for producing 7-MX using unstable plasmid-based *E. coli* chassis **(Fig. S21)** and recorded a low E-factor and PMI values, indicating greener synthesis (**Fig. 6D, Table S11**) [13, 14, 38]. The implemented coupling of the N-demethylation reaction with redox balance minimizes the titer gap in achieving methylated xanthines at the highest reported levels to date. This approach was systematically designed to reduce the metabolic burden on the cells, distinguishing it from other studies. Understanding this concept will be crucial for the rational engineering of biocatalysts for N-demethylation, which extends beyond just the production of 7-methylxanthine. Collectively, we demonstrated the systematic development of a robust *P. putida* biocatalyst and process for the green synthesis of high-value methylxanthines from caffeine in a techno-economically feasible manner.

Author contributions

LNJ conceptualized and designed the study, leading the funding acquisition, writing, and editing of the overall manuscript. BJ spearheaded the design and execution of the experiments and contributed to the initial draft of the manuscript. RMS and SZ conducted the biochemical assays to characterize feedback inhibition. GM led the TEA and LCA analyses for the process. All authors contributed to drafting and editing the manuscript.

Conflicts of interest

LNJ and BJ have filed a patent application (US 63/539,644) on the strains described in this manuscript.

Data availability

Supplementary information for this paper is available at https://doi.org/xxx; The online version contains extended data and supplementary material. Data supporting the findings of this study are available and deposited in digital format and can be distributed upon request. The engineered strains and plasmids developed in this study can only be provided for non-commercial purposes, as they are of commercial interest.

Acknowledgments

This work was supported by Green Core LLC, Japan, under the project "Green Tea for Green Plastic" (Project grant number C-22-0027). We would also like to acknowledge the SIUC NSF Research Experiences for Undergraduates program for supporting Kara Rollins and Joshua Lopez (Project grant number DMR 1757954), who conducted the shake flask experiments for this initial study. We thank Ian Brown and River Copeland for their help with biochemical assays (feedback inhibition).

References

View Article Online
DOI: 10.1039/D5GC02883C

1. L.-F. Hung, B. Arumugam, L. Ostrin, N. Patel, K. Trier, M. Jong and E. L. Smith III, *Investigative ophthalmology & visual science*, 2018, **59**, 472–486.
2. L. Lai, K. Trier and D.-M. Cui, *International Journal of Ophthalmology*, 2023, **16**, 969.
3. I.-A. Lee, A. Kamba, D. Low and E. Mizoguchi, *World Journal of Gastroenterology: WJG*, 2014, **20**, 1127.
4. K. Trier, D. Cui, S. Ribel-Madsen and J. Guggenheim, *British Journal of Ophthalmology*, 2023, **107**, 1538–1544.
5. H. Nonaka, M. Ichimura, M. Takeda, Y. Nonaka, J. Shimada, F. Suzuki, K. Yamaguchi and H. Kase, *European Journal of Pharmacology: Molecular Pharmacology*, 1994, **267**, 335–341.
6. M. McKeague, Y.-H. Wang, A. Cravens, M. N. Win and C. D. Smolke, *Metabolic engineering*, 2016, **38**, 191–203.
7. A. Gulevskaya and A. Pozharskii, *Chemistry of Heterocyclic compounds*, 1991, **27**, 1–23.
8. R. He, S. M. Ching and Y. Lam, *Journal of combinatorial chemistry*, 2006, **8**, 923–928.
9. A. Kapri, N. Gupta and S. Nain, *Scientifica*, 2022, **2022**, 8239931.
10. I. A. Zavialov, V. H. Dahanukar, H. Nguyen, C. Orr and D. R. Andrews, *Organic letters*, 2004, **6**, 2237–2240.
11. M. B. Allwood, B. Cannan, D. M. van Aalten and I. M. Eggleston, *Tetrahedron*, 2007, **63**, 12294–12302.
12. J. A. MONTGOMERY and K. HEWSON, *The Journal of Organic Chemistry*, 1961, **26**, 4469–4472.
13. M. B. Mock and R. M. Summers, *Journal of Biological Engineering*, 2023, **17**, 2.
14. M. B. Mock, A. Cyrus and R. M. Summers, *Biotechnology and Bioengineering*, 2022, **119**, 3326–3331.
15. E. M. Quandt, R. M. Summers, M. V. Subramanian and J. E. Barrick, *Genome Announcements*, 2015, **3**, 10.1128/genomea. 00640–00615.
16. J. H. Kim, B. H. Kim, S. Brooks, S. Y. Kang, R. M. Summers and H. K. Song, *Journal of Molecular Biology*, 2019, **431**, 3647–3661.
17. R. M. Summers, J. L. Seffernick, E. M. Quandt, C. L. Yu, J. E. Barrick and M. V. Subramanian, *Journal of bacteriology*, 2013, **195**, 3933–3939.
18. C. Liu, Y. Wu, H. Zhao, X. Gu, J. Gu, M. Zhao, S. Zuo and P. Wang, *ACS Sustainable Chemistry & Engineering*, 2024, **12**, 9716–9726.
19. M. B. Mock, S. B. Mills, A. Cyrus, H. Campo, T. Dreischarf, S. Strock and R. M. Summers, *Biotechnology and Bioprocess Engineering*, 2022, **27**, 640–651.
20. E. Martínez-García and V. de Lorenzo, *Current opinion in biotechnology*, 2024, **85**, 103025.
21. E. Martínez-García, P. I. Nikel, T. Aparicio and V. de Lorenzo, *Microbial cell factories*, 2014, **13**, 1–15.
22. L. N. Jayakody, C. W. Johnson, J. M. Whitham, R. J. Giannone, B. A. Black, N. S. Cleveland, D. M. Klingeman, W. E. Michener, J. L. Olstad and D. R. Vardon, *Energy & Environmental Science*, 2018, **11**, 1625–1638.
23. M. A. Franden, L. N. Jayakody, W.-J. Li, N. J. Wagner, N. S. Cleveland, W. E. Michener, B. Hauer, L. M. Blank, N.

Wierckx and J. Klebensberger, *Metabolic engineering*, 2018, **48**, 197–207.
24. R. M. Summers, T. M. Louie, C.-L. Yu, L. Gakhar, K. C. Louie and M. Subramanian, *Journal of bacteriology*, 2012, **194**, 2041–2049.
25. J. Ziegenhorn, M. Senn and T. Bücher, *Clinical chemistry*, 1976, **22**, 151–160.
26. I. De Marco, S. Riemma and R. Iannone, *The Journal of Supercritical Fluids*, 2018, **133**, 393–400.
27. M. A. Huijbregts, Z. J. Steinmann, P. M. Elshout, G. Stam, F. Verones, M. Vieira, M. Zijp, A. Hollander and R. Van Zelm, *The international journal of life cycle assessment*, 2017, **22**, 138–147.
28. R. E. James III, S. Leptinsky and M. Turner, *Quality Guidelines for Energy System Studies-Capital Cost Scaling Methodology: Revision 4a Report*, National Energy Technology Laboratory (NETL), Pittsburgh, PA, Morgantown, WV …, 2022.
29. F. K. Kazi, J. Fortman, R. Anex, G. Kothandaraman, D. Hsu, A. Aden and A. Dutta, *Techno-economic analysis of biochemical scenarios for production of cellulosic ethanol*, National Renewable Energy Lab.(NREL), Golden, CO (United States), 2010.
30. R. A. Sheldon, *Green Chemistry*, 2017, **19**, 18–43.
31. C. Jimenez-Gonzalez, C. S. Ponder, Q. B. Broxterman and J. B. Manley, *Organic Process Research & Development*, 2011, **15**, 912–917.
32. G. P. Da Silva, M. Mack and J. Contiero, *Biotechnology advances*, 2009, **27**, 30–39.
33. C. R. Amendola, W. T. Cordell, C. M. Kneucker, C. J. Szostkiewicz, M. A. Ingraham, M. Monninger, R. Wilton, B. F. Pfleger, D. Salvachúa and C. W. Johnson, *Metabolic Engineering*, 2024, **81**, 88–99.
34. I. F. Escapa, C. Del Cerro, J. L. García and M. A. Prieto, *Environmental Microbiology*, 2013, **15**, 93–110.
35. P. I. Nikel, J. Kim and V. De Lorenzo, *Environmental microbiology*, 2014, **16**, 239–254.
36. J. R. Elmore, A. Furches, G. N. Wolff, K. Gorday and A. M. Guss, *Metabolic engineering communications*, 2017, **5**, 1–8.
37. X. Chen, S. Li and L. Liu, *Trends in biotechnology*, 2014, **32**, 337–343.
38. C. Liu, Y. Wu, H. Zhao, X. Gu, J. Gu, M. Zhao, S. Zuo and P. Wang, *ACS Sustainable Chemistry & Engineering*, 2024.
39. A. Roca, J. J. Rodríguez-Herva and J. L. Ramos, *Journal of bacteriology*, 2009, **191**, 3367–3374.
40. A. Roca, J. J. Rodríguez-Herva, E. Duque and J. L. Ramos, *Microbial Biotechnology*, 2008, **1**, 158–169.
41. N. Tanaka, Y. Kusakabe, K. Ito, T. Yoshimoto and K. T. Nakamura, *Journal of molecular biology*, 2002, **324**, 519–533.
42. K. H. Algharrawi, R. M. Summers, S. Gopishetty and M. Subramanian, *Microbial cell factories*, 2015, **14**, 1–12.
43. J. Jumper, R. Evans, A. Pritzel, T. Green, M. Figurnov, O. Ronneberger, K. Tunyasuvunakool, R. Bates, A. Žídek and A. Potapenko, *nature*, 2021, **596**, 583–589.
44. D. Li, Y. Ge, N. Wang, Y. Shi, G. Guo, J. Zhang, Q. Zou and Q. Liu, *Microbiology Spectrum*, 2024, **12**, e00111–00124.
45. H. Tsuchiya, S. Doki, M. Takemoto, T. Ikuta, T. Higuchi, K. Fukui, Y. Usuda, E. Tabuchi, S. Nagatoishi and K. Tsumoto, *Nature*, 2016, **534**, 417–420.
46. K. Shimizu and Y. Matsuoka, *Biotechnology Advances*, 2022, **55**, 107887.
47. M. B. Mock, S. Zhang, K. Pakulski, C. Hutchison, M. Kapperman, T. Dreischarf and R. M. Summers, *Journal of Biotechnology*, 2024, **379**, 25–32.
48. W. R. Henson, A. W. Meyers, L. N. Jayakody, A. DeCapite, B. A. Black, W. E. Michener, C. W. Johnson and G. T. Beckham, *Metabolic engineering*, 2021, **68**, 14–25.
49. L. R. Lynd, G. T. Beckham, A. M. Guss, L. N. Jayakody, E. M. Karp, C. Maranas, R. L. McCormick, D. Amador-Noguez, Y. J. Bomble and B. H. Davison, *Energy & Environmental Science*, 2022, **15**, 938–990.
50. D. Choe, J. H. Lee, M. Yoo, S. Hwang, B. H. Sung, S. Cho, B. Palsson, S. C. Kim and B.-K. Cho, *Nature communications*, 2019, **10**, 935.
51. M. Dragosits and D. Mattanovich, *Microbial cell factories*, 2013, **12**, 1–17.
52. A. Z. Werner, Y.-S. C. Avina, J. Johnsen, F. Bratti, H. M. Alt, E. T. Mohamed, R. Clare, T. D. Mand, A. M. Guss and A. M. Feist, *Metabolic Engineering*, 2025, **88**, 196–205.
53. Y. Wu, A. Jameel, X.-H. Xing and C. Zhang, *Trends in biotechnology*, 2022, **40**, 38–59.
54. A. I. Benítez-Mateos, D. Roura Padrosa and F. Paradisi, *Nature chemistry*, 2022, **14**, 489–499.
55. K. Ding, M. Chin, Y. Zhao, W. Huang, B. K. Mai, H. Wang, P. Liu, Y. Yang and Y. Luo, *Nature Communications*, 2024, **15**, 6392.
56. M. A. Kukurugya, C. M. Mendonca, M. Solhtalab, R. A. Wilkes, T. W. Thannhauser and L. Aristilde, *Journal of Biological Chemistry*, 2019, **294**, 8464–8479.
57. S. Hernández-Arranz, R. Moreno and F. Rojo, *Environmental microbiology*, 2013, **15**, 227–241.
58. A. Kahnert, P. Mirleau, R. Wait and M. A. Kertesz, *Environmental microbiology*, 2002, **4**, 225–237.
59. R. Moreno, M. Martínez-Gomariz, L. Yuste, C. Gil and F. Rojo, *Proteomics*, 2009, **9**, 2910–2928.
60. N. P. McNulty and J. I. Gordon, *Nature microbiology*, 2024, 1–2.
61. L. N. Jayakody, S. D. Hamilton-Brehm, K. B. Anderson, M. E. McCarroll, G. L. A. Baduge, P. Sivakumar, K. Majumder, I. M. Jasiuk and R. R. Tannenbaum, *Trends in Biotechnology*, 2024.
62. W.-J. Kim, J.-D. Kim, J. Kim, S.-G. Oh and Y.-W. Lee, *Journal of Food Engineering*, 2008, **89**, 303–309.

View Article Online
DOI: 10.1039/D5GC02883C

Data Availability Statement

Supplementary information for this paper is available at https://doi.org/xxx; The online version contains extended data and supplementary material. Data supporting the findings of this study are available and deposited in digital format and can be distributed upon request. The engineered strains and plasmids developed in this study can only be provided for non-commercial purposes, as they are of commercial interest.